NANO LETTERS

2004
Vol. 4, No. 9
1725−1731

Single-Walled Carbon Nanotube AFM Probes: Optimal Imaging Resolution of Nanoclusters and Biomolecules in Ambient and Fluid Environments

Liwei Chen,* Chin Li Cheung, Paul D. Ashby, and Charles M. Lieber

Department of Chemistry and Chemical Biology, Harvard University, Cambridge, Massachusetts 02138

Received June 30, 2004

ABSTRACT

Carbon nanotubes are potentially ideal atomic force microscopy (AFM) probes due to their well-defined geometry, robust mechanical properties, and in the case of single-walled nanotubes (SWNTs), diameters approaching the size of small organic molecules. Here we elucidate fundamental factors that determine AFM imaging resolution using a combination of experiments with well-characterized SWNT probes and numerical simulations. Tapping mode AFM imaging on gold nanoclusters and DNA molecules using SWNT probes shows that the tip-induced broadening reaches the geometrical limit (i.e., the diameter of the SWNT tips) in the repulsive imaging regime, and the broadening effect becomes greater than the geometrical limit in the attractive imaging regime due to long-range attractive forces. Adjusting the damping enables imaging of isolated DNA molecules with a resolution defined by the tip diameter without disrupting the sample.

Introduction. Atomic force microscopy (AFM) has played an important role in nanoscale science and technologies due to its unique capabilities of imaging and manipulating structures at the nanometer scales.[1−4] In AFM and other scanning probe microscopies, the probe tip is a critical and potentially limiting component of the overall technology. Conventional microfabricated pyramidal silicon tips and oxide-sharpened silicon nitride tips typically have radii of curvature that range from 5 to 15 nm, with half cone angles of 10−35°.[5] In many imaging applications, such as studies of nanostructures and isolated biological macromolecules, smaller and higher aspect ratio tips are needed.

The unique properties of carbon nanotubes and especially single-walled carbon nanotubes (SWNTs) can be exploited to overcome the limitations of conventional tips.[6,7] First, the diameter of SWNTs can be as small as 0.4 nm, which is comparable to small molecules.[8,9] Second, the cylindrical structure of carbon nanotubes makes it possible to image high aspect ratio samples.[10,11] Third, the extremely high Young's modulus of carbon nanotubes, 1 TPa,[12] results in low thermal vibrations, and thus enables very small diameter and high aspect ratio tubes to be sufficiently stable for imaging at room temperature. Fourth, carbon nanotubes can reversibly buckle under high load without wear, reducing damage to both the tip and the sample.[11−13] Last, the ends of carbon nanotube tips can be chemically modified for high-resolution functional imaging.[14,15] Recent developments have led to routine preparation of individual SWNT tips with diameters ranging from 0.8 nm to greater than 3 nm,[16−18] and thus open up the possibility of quantitative studies of factors that affect image resolution.

Previous studies using SWNT tips have enabled routine high-resolution imaging of nanoclusters and proteins, and protein−DNA complexes in tapping mode under ambient conditions.[10] The effect of the SWNT length and mechanical stability on image resolution on polycrystalline metal thin films and semiconductor nanocrystals has also been studied.[19,20] A recent paper correlated TEM characterization of nanotube tips with AFM images taken by the tips.[21] Based on simple geometric considerations that neglect potentially complex tip−sample interactions, the tip-induced broadening should be directly related to the size of the probe tip. However, a fundamental understanding of the effects of the tip size and tip−sample interaction on the observed resolution is yet not available. A rigorous analysis of the tip-broadening effect is not generally possible with conventional probes because (i) the radius of curvature varies considerably from tip to tip, (ii) tips are subject to wear during imaging, and (iii) the cone shape of conventional tips makes the tip broadening effect dependent upon the sample height. SWNT tips have cylindrical shape and have tip sizes similar to or even smaller than many nanometer-scaled structures, and thus are good systems with which to understand broadening effects from tip shape and tip−sample interactions.

* Corresponding author: Liwei Chen (current address) Department of Chemistry and Biochemistry, Ohio University, Athens, OH 45701; E-mail: lc2045@columbia.edu.

10.1021/nl048986o CCC: $27.50
Published on Web 07/24/2004

Experimental Section. *Individual SWNT Tip Preparation.* We prepared individual SWNT tips of different diameters by controlling the catalyst size in two previously reported methods: direct surface growth of carbon nanotubes on AFM tips[6] and the carbon nanotube "pick-up" method.[17] In the surface growth method, FeO_x colloid catalyst was deposited onto commercial silicon FESP probes (force modulation etched silicon probe, $k = 0.5-5$ N/m, Digital Instruments, Santa Barbara, CA), and the Si AFM probes were then placed in a chemical vapor deposition furnace for nanotube growth using conditions described previously.[6] In the pick-up method, $Fe(NO_3)_3$ catalyst was deposited on oxidized silicon substrates and individual nanotubes were grown near normal to the surface.[17] Commercial silicon AFM probes were used to scan the surface and "pick-up" single SWNTs. A thin layer of UV-curable glue (Loctite 3105) was used to coat the surface of Si probes and then cured under UV light (UVGL 23 Mineralight lamp, UVP, Inc.) after the nanotube was assembled to ensure good adhesion between the nanotubes and the Si probe in fluid imaging experiments.

The lengths of nanotube tips were adjusted for optimal imaging using a pulsed etching technique described previously.[17] Briefly, SWNT tips are used to image a highly n-doped silicon substrate while 50 μs pulses of 10−25 V are applied to the substrate with the tips grounded. The nanotubes were shortened roughly 2−5 nm per pulse.

Sample Preparation. A 1235 base pair linear DNA fragment obtained from AseI digestion of the pBS+ (Stratagene) phagemid was a gift from Karl A. Haushalter. The sample was purified with standard agarose gel extraction and then followed by ethanol precipitation. The resulting DNA was resuspended in 10 mM Tris buffer, pH 7.0. A deposition solution was made by mixing DNA with $MgCl_2$ to a final concentration of 0.5 nM DNA and 5mM Mg^{2+}. For AFM imaging in ambient, the deposition solution was applied to a freshly cleaved mica surface for 1 min before the mica sample was rinsed in water (OmniSolv. water, EM science, Gibbstown, NJ) and dried under a stream of N_2 gas. For AFM imaging in aqueous media, freshly cleaved mica was treated with 0.01% w/v poly-L-lysine (Ted Pella, Redding, CA) for 1 min, rinsed with water, dried, and then a drop of 0.5 nM DNA solution containing no Mg^{2+} was applied for 1 min. The mica sample was then rinsed and kept covered with pure water until the entire imaging experiment was finished.

Gold nanocluster samples with diameters of 5.2 ± 1 nm were prepared in a similar manner. All nanocluster diameters were approximated from heights obtained in topographical images. A freshly cleaved mica surface was treated with 0.01% w/v poly-L-lysine for 1 min, rinsed with water, and dried. A 5 μL portion of the 1:20 water diluted gold nanocluster (Ted Pella, Redding, CA) solution was deposited for 1 min. The mica surface was then rinsed with water and dried under dry nitrogen gas.

AFM. All AFM images were recorded in tapping mode with a Multimode Nanoscope IIIa microscope and an Extender module (Digital Instruments, Santa Barbara, CA) in aqueous solution or in air. For imaging in air, the SWNT tips fabricated from FESP tips were excited at resonance frequencies around 70 kHz with free amplitude of 5−40 nm. In aqueous solution, the resonance peak of an FESP probe, which is usually broad ($Q = 3.8$) and centered at ca. 30 kHz, was excited by a fluid acoustic mode peak that overlaps with the true resonance peak; the free oscillation amplitude was typically 2−5 nm as calibrated by the amplitude force curves. The imaging amplitude (amplitude feedback set point) for air and aqueous imaging were chosen from 40 to 90% of the free amplitude. The amplitude and phase signals of the cantilever oscillation as a function of tip−sample separation, which are denoted as force calibration curves (FCs) hereafter, were recorded for different imaging conditions. The manufacturer-defined phase signal, which is specific only to the Nanoscope Extender module, was converted to the conventional phase defined as zero on resonance by the equation

$$\text{phase lag (convention)} = \cos^{-1}(\text{phase lag (extender recorded)}/90^\circ) \quad (1)$$

Transmission Electron Microscopy. AFM cantilever/tip assemblies with nanotube tips were mounted on a custom transmission electron microscope (TEM) holder and imaged with a Philips EM420 (FEI, Hillsboro, OR) TEM operated at 100 kV.

Simulation of AFM Tip Dynamics. The dynamics of the AFM tip was simulated by numerically solving the nonlinear, second-order differential equation of motion.[22] The equation of motion includes the elastic response of the cantilever, the hydrodynamic damping of the medium, the tip−sample interaction and the sinusoidal driving force:

$$m\frac{\mathrm{d}z^2}{\mathrm{d}^2t} = -kz - \frac{m\omega_0}{Q}\frac{\mathrm{d}z}{\mathrm{d}t} + F_{\mathrm{int}} + F_0\cos\omega t \quad (2)$$

where m, k, ω_0, Q are the effective mass, spring constant, resonance frequency, and quality factor of the cantilever resonance, respectively; z is the vertical displacement of the tip from base of the cantilever; ω and F_0 are the frequency and the amplitude of the driving force, respectively; and F_{int} is the tip−sample interaction force experienced by the tip.

For simulations of cantilever dynamics in solution, the tip−sample interaction is modeled by van der Waals forces before the tip−sample contact and Derjaguin-Müller-Toporov (DMT) contact mechanics,[23] which combines the adhesion forces with the Pauli and ionic repulsion, after contact.

$$F_{\mathrm{int}} = \begin{cases} -\dfrac{HR}{6z^2} & z > a_0 \\ -\dfrac{HR}{6a_0^2} + \dfrac{4}{3}E^*\sqrt{R}(a_0 - z)^{3/2} & z < a_0 \end{cases} \quad (3)$$

In eq 3, E^* is the reduced Young's modulus, H is the Hamaker constant, R is the tip radius, a_0 is the DMT adhesion radius determined by

$$F_a = 4\pi R\gamma = \frac{HR}{6a_0^2} \quad (4)$$

where F_a is the adhesion force and γ is the interfacial energy.

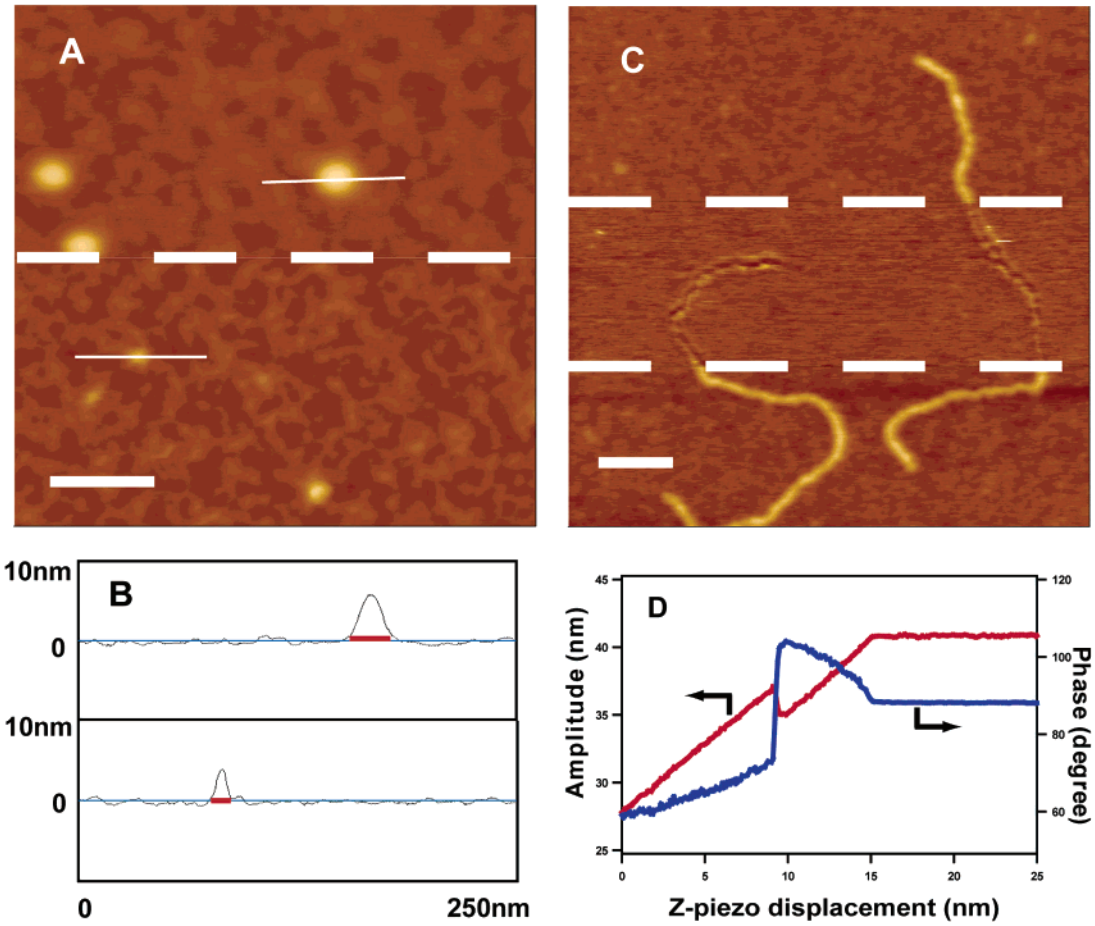

Figure 1. (A) Gold nanoclusters imaged with SWNT tips in ambient conditions with a free oscillation amplitude (A_0) of 40 nm. The top section above the thick white dashed boundary line was imaged with an amplitude set point (A_{sp}) of 37 nm, whereas the bottom section was imaged with an A_{sp} of 26 nm. The scale bar is 50 nm. The narrow white lines indicate the direction of the height cross sections shown in B. (B) The height cross sections of the gold nanoclusters in image A. The top trace corresponds to the nanocluster in the top section of image A and the bottom trace corresponds to the nanocluster in the bottom section of the image. (C) Isolated DNA molecules imaged with SWNT tips in ambient with an A_0 of 42 nm. The top and bottom section were imaged with an A_{sp} of 38 nm, whereas the midsection was imaged with an A_{sp} of 32 nm. The scale bar is 50 nm. (D**)** Force calibration (FC) curves of the amplitude and phase channels for a SWNT tip imaging in ambient with an A_0 of 42 nm.

For cantilever in ambient conditions, the van der Waals interaction is not adequate to describe the tip sample interaction because the attractive interaction is dominated by capillary forces. A decaying exponential is used to model the noncontact capillary forces. The DMT mechanics is used for the interaction after contact.

$$F_{\text{int}} = \begin{cases} -Ae^{-z/d} & z > 0 \\ -A + \frac{4}{3}E^*\sqrt{R}(-z)^{3/2} & z < 0 \end{cases} \quad (5)$$

where A is the preexponential factor for the attractive forces and d is a decay constant.

The equation of motion (eq 2) was solved numerically as the sample gradually "moved" toward the cantilever. All simulations were performed driving at the resonance. The oscillation amplitude, phase shift, and average tip−sample interaction force were calculated from the time trajectories. The radius of carbon nanotube tips and the spring constant of the FESP cantilever were set to typical values of 2 nm and 1 N/m, respectively. Since the Young's modulus of carbon nanotube is ca. 1 TPa,[12] the reduced Young's modulus E^* is dominated by the mica surface (2GPa) when the SWNT tip contacts the surface vertically. In air, the parameters were: resonance frequency 75 kHz, $Q = 60$, as obtained in experiments. The preexponential factor (A) 3 nN and the decay constant (d) 0.5 nm for the capillary forces were based on the contact mode force curves and adjusted to reproduce experimental cantilever dynamics. In aqueous solution, the parameters used in the simulation were: resonance frequency 30 kHz, $Q = 3.8$ (measured from thermal spectrum), and Q $= 50$ (elevated value with controlled Q factor). The Hamaker constant, 0.83×10^{-20} J, was based on the quartz−quartz value in water.[24] The surface energy, 9 mJ/m^2, was determined from experimental adhesion force, using DMT contact mechanics (eq 4).

Results. *Carbon Nanotube Probe Imaging in Air.* Two distinct imaging regimes that are characterized by drastically different resolutions are observed in air using SWNT tips at high free oscillation amplitude, A_0 (Figure 1). In the top half of Figure 1A, a 6 nm diameter gold nanocluster is imaged by a SWNT tip with an A_0 of 40 nm and an amplitude set point (A_{sp}) of 37 nm. The tip diameter of this particular

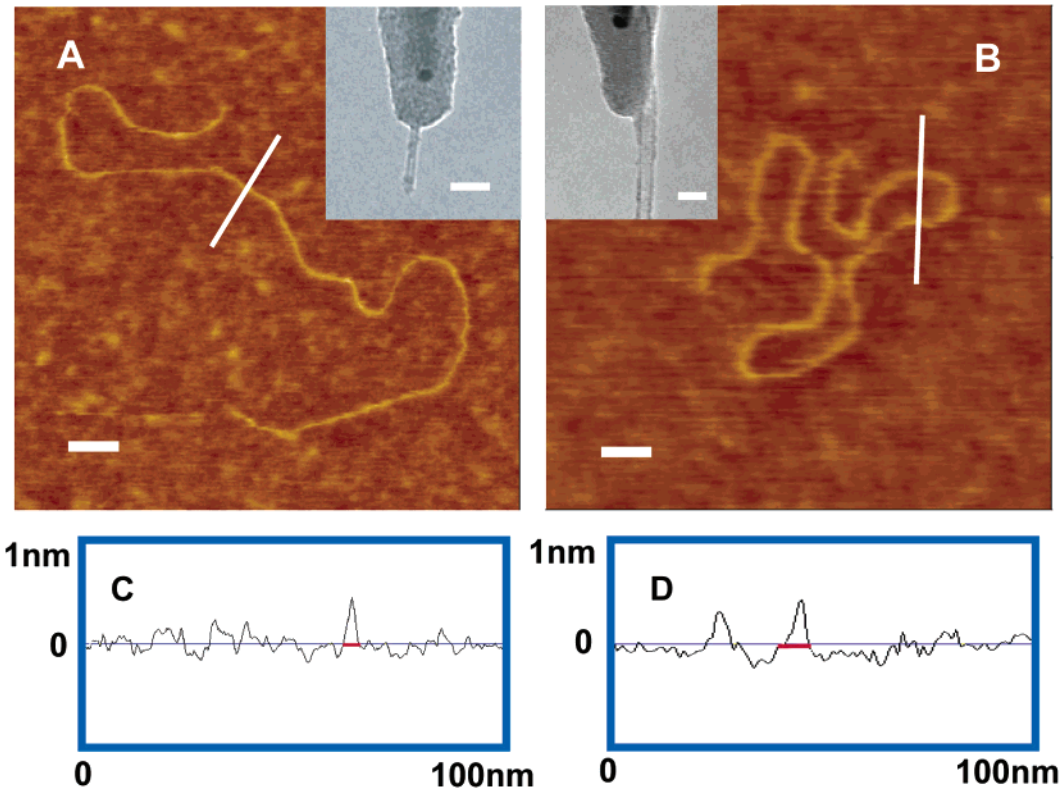

Figure 2. (A and B) Isolated DNA molecules imaged with SWNT tips in water. Insets are TEM images of the corresponding SWNT tips used to obtain the AFM images in A and B, with tip diameters of 2.4 and 5.8 nm, respectively. The scale bars are 20 nm for the AFM images, and 10 nm for the insets. (C and D) The cross sections of the DNA imaged in A and B with full widths of 4.5 ± 0.2 nm and 8.0 ± 0.3 nm, respectively (the average width and standard deviations are obtained from 6 measurements).

SWNT probe is measured by TEM to be 3.5 nm. The full width of the gold particle appears to be 26 nm from the cross section (Figure 1B). The bottom half of Figure 1A is captured in the same scan using identical imaging conditions except for one parameter: set-point amplitude. Changing the A_{sp} from 37 to 26 nm leads to a substantially reduced apparent full width of 10 nm for the gold particles (Figure 1B). The resolution obtained in this second regime agrees with predictions based on simple geometric considerations: the 10 nm apparent full width is the sum of the true nanocluster diameter (6 nm) and the diameter of the SWNT tip (3.5 nm).

Biological macromolecules are usually much softer and more prone to mechanical deformation than inorganic samples such as the metal nanoclusters studied above. Therefore, we imaged isolated DNA molecules as a model system in order to investigate the role of sample elasticity on image resolution. Typical images of DNA recorded using an A_0 of 42 nm also exhibit the two distinct regimes as shown in Figure 1C. The top and bottom sections of Figure 1C, which were obtained with a high A_{sp} of 38 nm, exhibit a full width of 12 nm, much larger than the sum of the diameters of the DNA (2 nm) and the nanotube (3−4 nm). On the other hand, the DNA image in the middle section of Figure 1C, which was obtained with a low A_{sp} of 32 nm, is highly distorted. This highlights how low sample stiffness significantly limits AFM image resolution in ambient conditions.

In contrast to the two distinct imaging regimes observed above with high A_0 of 40 nm, only one imaging regime is observed when a low A_0 of 10 nm is used. At such low A_0, no drastic difference in image resolution is seen when A_{sp} is adjusted through the 20−99% range of the A_0. The images look similar to those obtained in the high A_{sp} regime using high A_0 on both the gold nanocluster and DNA samples (data not shown), and the full width of the sample features appears to be much greater than the sum of the true width and the nanotube diameter.

Force curves that record the tip oscillation amplitude and phase as a function of the tip−sample distance are key to understanding factors that affect resolution during tapping mode imaging. As shown in Figure 1D, the oscillation amplitude first decreases linearly when the tip approaches the sample with a high A_0 of 42 nm; and the corresponding phase of the tip oscillation gradually increases. When the tip reaches a position approximately 9 nm away from the surface, the amplitude jumps from 35 to 37 nm and the phase signal drops from 105° to 75°. This rapid transition in both the amplitude and phase of the tip oscillation phenomenologically accounts for the transition between the two distinct regimes observed in imaging experiments.

Carbon Nanotube Probes Imaging in Fluid. Figure 2A and 2B show images of isolated DNA molecules obtained in aqueous environment using SWNT tips of different diameters. Only one imaging regime is seen in aqueous imaging. The FC in aqueous environment reveals a monotonic decrease in both amplitude and phase channel, with the phase lag signal always smaller than 90° (data not shown).

The apparent full width of the DNA double helix in aqueous imaging shows a direct scaling with the tip diameter.

Cross-sections taken from images show that the full width of a DNA double helix (true width 2 nm) becomes 4.3 nm when imaged with a 2.4 nm nanotube tip (Figure 2C) and 8.0 nm when imaged with a 5.8 nm nanotube tip (Figure 2D). The geometry-limited tip-broadening of the DNA in Figure 2 and the phase angle less than 90° suggest that imaging in aqueous conditions belongs to the same regime as in ambient conditions with high A_0 and low A_{sp}, even though the free oscillation amplitude in aqueous environment (2−5 nm) is extremely low compared to that in ambient (40 nm).

Cantilever Dynamics and the Tip−Sample Interaction. The cantilever equation of motion (eq 2) is numerically solved to produce cantilever time trajectories. The tip oscillation amplitude and phase are extracted from each trajectory and plotted as a function of tip−sample separation. The tip−sample interaction force is obtained by averaging over 100 oscillation cycles (200 points per cycle evenly distributed in time) after the cantilever reaches steady states at each tip−sample distance.

Solutions of the equation of motion (eq 2) for parameters corresponding to ambient conditions (Figure 3A) qualitatively reproduce the FCs obtained in experiments (Figure 1D). The oscillation amplitude first sees a linear decrease and then undergoes a sudden jump followed by linear decrease again. Correspondingly, the phase signal first gradually increases and then displays a discontinuous transition from > 90° to < 90°. These features show excellent agreement with the experiments and demonstrate that the simulation reliably captures the essence of the cantilever dynamics. More importantly, the simulation reveals the nature of the tip−sample interaction. As seen in Figure 3A, the averaged tip−sample interaction is attractive in the high A_{sp} regime and it becomes repulsive in the low A_{sp} regime. The transition from attractive to repulsive interaction coincides with the transition in amplitude and phase FCs.

Simulations of the aqueous experiments (Figure 3B blue trace) show a steady decrease in both the amplitude and the phase (always < 90°) throughout the entire FC, which agree with the experiments. The tip−sample interaction is repulsive under these conditions.

The major differences between imaging in ambient and in fluid are the cantilever resonance frequency and hydrodynamic damping. We studied the damping effect by changing the quality factor, Q, while keeping all other parameters identical except that the driving force is lowered to keep the same free oscillation amplitude. Solutions for fluid imaging parameters with an elevated Q of 50 (Figure 3B red trace) show an obvious transition in phase from a value greater than 90° to smaller than 90°. The two corresponding regimes can also be seen in the amplitude FC, although the high A_{sp} regime is very narrow in range. At the same tip−sample distance, the cantilever oscillation amplitude drops more with a high Q compared to that with a low Q. The tip−sample interaction also shows a narrow range of attractive force and a dominant repulsive force regime. Importantly, the average force between the tip and sample is 1 order of magnitude lower in the high Q simulation.

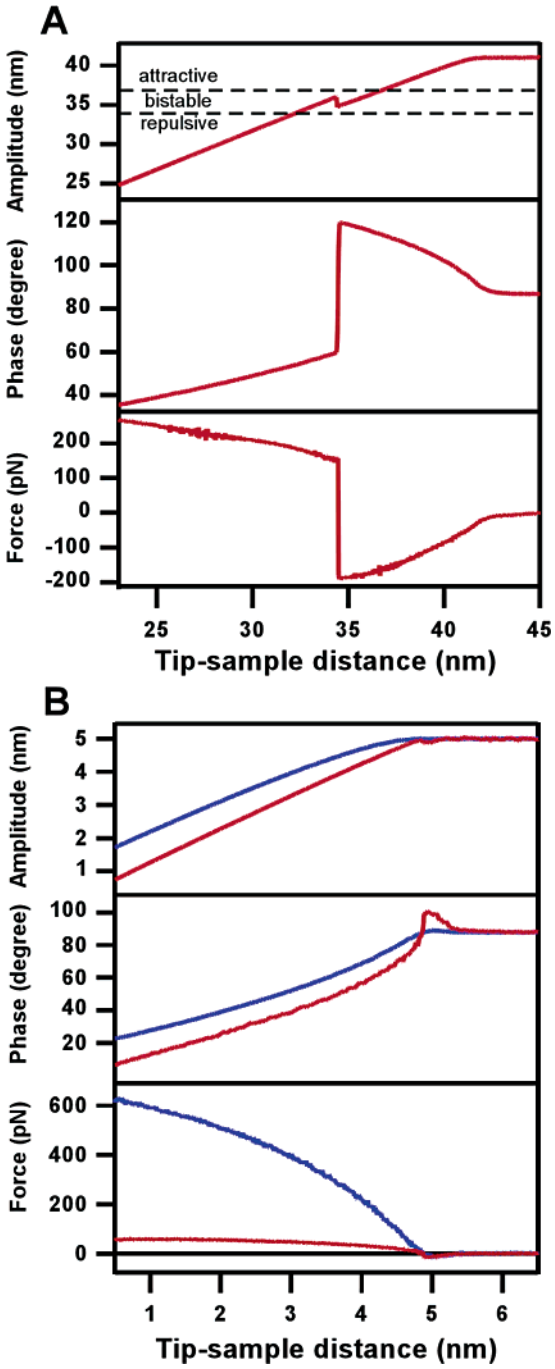

Figure 3. (A) Simulated force curves for SWNT tips imaging in ambient conditions. (B) Simulated force curves for SWNT tips imaging in aqueous environment. The blue trace is the solution for a Q factor of 3.8 (experimental value) and the red trace is the solution for an elevated Q of 50.

Discussion. *Repulsive and Attractive Regimes of Imaging.* SWNT tip tapping mode imaging in air with high free oscillation amplitude reveals two regimes. The two imaging regimes distinguish themselves by image quality and drastically different tip-induced broadening effect. In the high set point regime, the tip broadening is much greater than the SWNT tip diameter; on the other hand, the tip broadening is much reduced and equal to the SWNT diameter in the low set point regime. The realization of minimal tip broadening for stiff materials is of significant importance

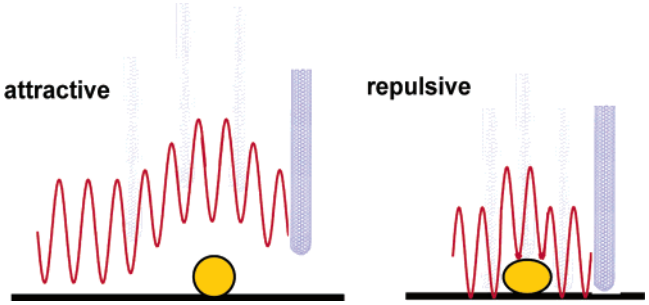

Figure 4. Illustration of the tip dynamics for SWNT probe imaging in attractive and repulsive regimes.

for nanodevice structural characterization. The well-defined and predictable resolution would allow accurate deconvolution of the image. At the same time, our studies highlight the challenge for ultrahigh resolution imaging of soft materials such as biological macromolecules in ambient. As shown in Figure 1C, the DNA images in the low set point regime are greatly distorted.

Numerical simulation of the cantilever dynamics qualitatively reproduced the existence of the two regimes. The tip−sample interaction as a function of distance as shown in Figure 3A indicates a fundamental difference between the two regimes that it is attractive in the high set point regime but repulsive in the low set point regime. This result explains the drastic difference in image resolution between the two regimes (Figure 4). In the attractive regime, tip-induced broadening is larger than the size of the SWNT probes because attractive interaction between the tip and sample is long range. In the repulsive regime, the tip probes the repulsion that is dictated by Pauli's exclusion principle, which closely resembles the geometric shape of the sample. The attractive interaction in air is most likely dominated by capillary forces. As a result of balancing the interfacial energies among the sample, substrate, and the air in the asymmetric geometry, it is conceivable to have a thick moisture condensation layer at the side of the nanoparticles but a rather thin layer on the top. Thus, the particle height in the attractive regime correlates poorly with the width and is in fact close to the true height of the particle.

The two imaging regimes have previously been observed in tapping mode under ambient conditions with high spring constant cantilevers ($k = 25-50$ N/m).[25] A direct correlation between the tip broadening and the tip size was not possible in these studies because of the ambiguity in tip size and shape. The authors recommended imaging in the attractive regime because a soft biological macromolecule, immunoglobulin G, showed irreversible deformation in the repulsive regime under their conditions. On the contrary, we suggest the repulsive regime for quantitative imaging because the attractive regime images can only be interpreted qualitatively. For hard samples such as the nanoclusters in Figure 1A, repulsive imaging conditions give minimum tip-induced broadening in full width of the features. Soft DNA molecules appear distorted under the repulsive regime in air (Figure 1C). This could be due to true mechanical distortion under repulsive forces and/or an artifact of strong disturbance in cantilever dynamics when the tip moves from a stiff substrate to a soft molecule. In either case, the repulsive regime in air is not well-suited for accurate structural imaging of biological molecules. A much less invasive method for imaging these soft materials in the repulsive regime will be addressed later in the discussion.

Cantilever Dynamics and Resonance Frequency Shift. When the tip is far away from the sample surface, the tip−sample interaction is negligible and the solution to the equation of motion (eq 2) is a driven damped oscillator with steady-state amplitude response A_0:

$$A_0 = \frac{F_0/m}{\sqrt{(\omega^2 - \omega_0^2)^2 + (\omega\omega_0/Q)^2}} \qquad (6)$$

As the tip approaches the sample, the nonlinear tip−sample interaction force term in equation 2 becomes important. Qualitatively, attractive force gradients act against the restoring force of the cantilever and thus effectively weaken the spring and lower the cantilever resonance frequency. On the other hand, repulsive force gradients effectively strengthen the spring and shift the cantilever resonance to the high-frequency side. When the tip approaches the sample from far away, the tip oscillation first falls into the attractive regime because the tip−sample interaction is attractive in the long range throughout the oscillation cycle. The attractive interactions shift the resonant frequency lower and, since the oscillation frequency is fixed by the AC drive, the oscillation amplitude decreases because the drive frequency is now off resonance.

An abrupt transition from the attractive to the repulsive regime occurs when the cantilever moves closer to the sample and starts to experience repulsive force gradient at the bottom of each oscillation cycle. The repulsive force gradient contributes to an increase in the effective spring constant and resonance frequency. Since the cantilever resonance is offset to lower frequency than the AC drive signal due to the overall attractive forces, the slight increase in resonance frequency means less offset resonance and increased amplitude. The increased amplitude in turn leads to more repulsive force gradient at the bottom of each cycle, which starts a loop of further increases in resonance frequency and repulsive force gradients. This positive feedback loop does not stop until the effective resonance moves to a point higher than the drive frequency and the system enters the stable repulsive regime with an effective resonance greater than the intrinsic cantilever resonance.

Aqueous Fluid Imaging and the Effect of Quality Factor. Figure 2 shows that there exists only one regime for SWNT tip imaging in aqueous tapping mode, despite the small oscillation amplitude. Three evidences suggest that the tip−sample interaction in this imaging regime is repulsive. First, the phase signal is smaller than 90°. Second, the tip-induced broadening effect is defined by the SWNT tip diameter. Third, the simulation (Figure 3B) using aqueous imaging parameters verifies the repulsive interaction between the tip and the sample.

AFM characterization at the single-molecule level with resolution down to a few nanometers is critical in identifying

global structural features for large protein−protein and protein−DNA complexes that are difficult to crystallize.[10,26] The ability to achieve minimal and well-defined tip-induced broadening while imaging soft macromolecules without damaging the soft materials has important implications for biology and macromolecular chemistry.

Although the major component of long-range attractive forces, capillary wetting, is eliminated in water, the very low driving frequency and much increased hydrodynamic damping are more important factors in determining the cantilever dynamics in aqueous environment. Simulation at an elevated quality factor of 50, which corresponds to about half of the media damping in reality, indeed indicates a very narrow attractive regime at large *z*-piezo distances. Throughout the force curve, simulation with the elevated quality factor results in smaller oscillation amplitude. Interestingly, the corresponding repulsive forces between the tip and sample also drop by almost an order of magnitude. We thus believe that active *Q* control may lead to less invasive imaging in the repulsive regime.[27]

In general, imaging of soft biomolecules is better achieved by imaging in solution to eliminate the attractive capillary forces, which requires large tapping amplitude to reach the repulsive regime. An electronically increased *Q* would reduce the interaction forces; therefore, the *Q* factor should be as large as possible without compromising stability or imaging speed.

Single-Walled Carbon Nanotube AFM Probes. We have shown that the repulsive regime of imaging needs to be accessed to achieve optimal and quantitative resolution. In general, high free oscillation amplitude and low amplitude set point lead to the repulsive imaging in air, which constitutes appropriate conditions for imaging hard materials. On the other hand, a few nanometers oscillation amplitudes in aqueous fluid also result in repulsive but noninvasive imaging, even for soft materials.

SWNT tips further benefit AFM imaging by favoring the cantilever dynamics in the repulsive regime in addition to apparent advantages such as small probe size and high aspect ratio. The small tip radius and high aspect ratio greatly reduce the attractive interaction forces between the tip and sample in both fluid and ambient conditions. This allows the cantilever dynamics to be in repulsive more easily so that smaller amplitudes can be used to preserve sample integrity. This is especially evident when tapping in ambient conditions where the wicking effect of the capillary force dominates the attractive interaction, making it both strong and long-range. Similarly, the advantages of nanotube tips are augmented by the hydrophobic nature of the probe, which further reduces the attractive interactions when interacting with the water layer in ambient conditions. Thus, the properties of nanotube probes make them ideal for imaging samples in the repulsive regime for high resolution in either solution or ambient conditions.

Conclusion. We have elucidated the fundamental factors determining image resolution in aqueous and ambient tapping mode AFM using well-characterized individual SWNT AFM probes with different diameters. A fine interplay among cantilever resonance frequency, quality factor, and tip and sample mechanical properties determines the cantilever dynamics. In the repulsive regime, the tip-induced broadening reaches the geometric limit; that is, the diameter of the SWNT tips. In attractive regime, the tip-broadening effect is dominated by long-range attractive interactions and yields much larger AFM image dilation. These results clearly indicate that the repulsive regime is necessary for quantitative imaging and analysis.

Acknowledgment. We thank Dr. Karl A. Haushalter for providing DNA samples and Dr. Jason Hafner for sharing experiences in SWNT tip preparation. The work was supported by the National Institutes of Health and the Air Force Office of Scientific Research.

References

(1) Giessibl, F. J. *Rev. Mod. Phys.* **2003**, *75*, 949−983.
(2) Horber, J. K. H.; Miles, M. J. *Science* **2003**, *302*, 1002−1005.
(3) Vettiger, P.; Cross, G.; Despont, M.; Drechsler, U.; Durig, U.; Gotsmann, B.; Haberle, W.; Lantz, M. A.; Rothuizen, H. E.; Stutz, R.; Binnig, G. K. *IEEE Trans. Nanotechnol.* **2002**, *1*, 39−55.
(4) Noy, A.; Vezenov, D. V.; Lieber, C. M. *Annu. Rev. Mater. Sci.* **1997**, *27*, 381−421.
(5) Product data sheets from manufacturer website: http://www.veeco.com
(6) Cheung, C. L.; Hafner, J. H.; Lieber, C. M. *Proc. Natl. Acad. Sci. U.S.A.* **2000**, *97*, 3809−3813.
(7) Hafner, J. H.; Cheung, C. L.; Lieber, C. M. *Nature (London)* **1999**, *398*, 761−762.
(8) Qin, L.-C.; Zhao, X.; Hirahara, K.; Miyamoto, Y.; Andos, Y.; Iijima, S. *Nature (London)* **2000**, *408*, 50.
(9) Wang, N.; Tang, Z. K.; Li, G. D.; Chen, J. S. *Nature (London)* **2000**, *408*, 50−51.
(10) Hafner, J. H.; Cheung, C.; Woolley, A. T.; Lieber, C. M. *Prog. Biophys. Mol. Biol.* **2001**, *77*, 73−110.
(11) Dai, H. J.; Hafner, J. H.; Rinzler, A. G.; Colbert, D. T.; Smalley, R. E. *Nature* **1996**, *384*, 147−150.
(12) Wong, E. W.; Sheehan, P. E.; Lieber, C. M. *Science* **1997**, *277*, 1971−1975.
(13) Iijima, S.; Brabec, C.; Maiti, A.; Bernholc, J. *J. Chem. Phys.* **1996**, *104*, 2089−2092.
(14) Wong, S. S.; Woolley, A. T.; Joselevich, E.; Cheung, C. L.; Lieber, C. M. *J. Am. Chem. Soc.* **1998**, *120*, 8557−8558.
(15) Wong, S. S.; Joselevich, E.; Woolley, A. T.; Cheung, C. L.; Lieber, C. M. *Nature (London)* **1998**, *394*, 52−55.
(16) Hafner, J. H.; Cheung, C. L.; Lieber, C. M. *J. Am. Chem. Soc.* **1999**, *121*, 9750−9751.
(17) Hafner, J. H.; Cheung, C.-L.; Oosterkamp, T. H.; Lieber, C. M. *J. Phys. Chem. B* **2001**, *105*, 743−746.
(18) Yenilmez, E.; Wang, Q.; Chen, R. J.; Wang, D. W.; Dai, H. J. *Appl. Phys. Lett.* **2002**, *80*, 2225−2227.
(19) Nguyen, C. V.; Chao, K. J.; Stevens, R. M. D.; Delzeit, L.; Cassell, A.; Han, J.; Meyyappan, M. *Nanotechnology* **2001**, *12*, 363−367.
(20) Snow, E. S.; Campbell, P. M.; Novak, J. P. *Appl. Phys. Lett.* **2002**, *80*, 2002−2004.
(21) Wade, L. A.; Shapiro, I. R.; Ma, Z. Y.; Quake, S. R.; Collier, C. P. *Nano Lett*. **2004**, *4*, 725−731.
(22) Garcia, R.; San Paulo, A. *Phys. Rev. B: Condens. Matter Mater. Phys.* **1999**, *60*, 4961−4967.
(23) Derjaguin, B. V.; Muller, V. M.; Toporov, Y. P. *J. Colloid Interface Sci.* **1975**, *53*, 314−326.
(24) Milling, A.; Mulvaney, P.; Larson, I. *J. Colloid Interface Sci*. **1996**, *180*, 460−465.
(25) Paulo, A. S.; Garcia, R. *Biophys. J.* **2000**, *78*, 1599−1605.
(26) Chen, L. W.; Haushalter, K. A.; Lieber, C. M.; Verdine, G. L. *Chem. Biol.* **2002**, *9*, 345−350.
(27) Rodriguez, T. R.; Garcia, R. *Appl. Phys. Lett.* **2003**, *82*, 4821−4823.

NL048986O